JOURNAL OF CATALYSIS **174,** 1–12 (1998)
ARTICLE NO. CA971890

Effects of 1,2 Dichloroethane Addition on the Optimal Silver Catalyst Distribution in Pellets for Epoxidation of Ethylene

King Lun Yeung,*[,1] Asterios Gavriilidis,*[,2] Arvind Varma,*[,3] and Madan M. Bhasin†

*Department of Chemical Engineering, University of Notre Dame, Notre Dame, Indiana 46556; and †Union Carbide Corporation, South Charleston, West Virginia 25303

Received November 14, 1996; revised September 2, 1997; accepted September 3, 1997

The issue of optimal catalyst distribution was studied experimentally for the ethylene epoxidation reaction network on a $Ag/\alpha\text{-}Al_2O_3$ catalyst in the presence of 1,2-dichloroethane (DCE). For a fixed amount of silver, the influence of location and width of the catalytic layer on the conversion of ethylene, and on the selectivity and yield to ethylene oxide, was investigated for different concentrations of DCE (0–2 ppm) using a single-pellet reactor. Two levels of ethane in the feed (0 and 0.5 vol%) and a temperature range between 210 and 270°C were studied. Depending on the experimental conditions, promotion, inhibition, and poisoning effects of DCE were observed. The catalyst distribution and the concentrations of DCE and ethane in the feed, which provide high selectivity and yield, were identified. XPS analysis was also conducted to determine the state and composition of the silver catalyst, both prior and subsequent to reaction.

INTRODUCTION

A number of theoretical and experimental studies have demonstrated that nonuniformly distributed catalysts can offer superior performance as compared to uniformly distributed catalysts. Some of the advantages include higher activity, selectivity, yield, durability, and thermal sensitivity. Wu *et al.* (1) examined the issue of optimal catalyst distribution in pellet for any performance index (conversion, selectivity, or yield) and for the most general case of an arbitrary number of reactions, following arbitrary kinetics, occurring in a nonisothermal pellet, with finite heat and mass transfer resistances. They showed analytically that the optimal distribution is a Dirac delta function; i.e., for optimal performance, the catalyst should be deposited at a specific location within the pellet. This location depends on the physicochemical parameters of the system, as well as on the performance index being maximized. The same conclusion was also reached for reaction systems with catalyst deactivation (2). In related work, Morbidelli *et al.* (3) have shown that the Dirac delta function can be approximated in practice by a narrow active layer with width less than 5% of the characteristic pellet dimension. A recent review of this subject has been published by Gavriilidis *et al.* (4).

A number of experimental studies have also been reported. They include CO oxidation over $Pt/\gamma\text{-}Al_2O_3$ pellets (5, 6), ethylene hydrogenation over $Pt/\gamma\text{-}Al_2O_3$ (7) and $Pd/\gamma\text{-}Al_2O_3$ (8), CO methanation over $Ni/\gamma\text{-}Al_2O_3$ (8, 9), and ethylene epoxidation over $Ag/\alpha\text{-}Al_2O_3$ (10) catalysts. In all cases, a catalyst pellet with a narrow active layer placed at the appropriate location offers the best conversion and selectivity values.

A previous study by Gavriilidis and Varma (10) has experimentally investigated the issue of optimal catalyst distribution for the ethylene epoxidation network. Their results clearly demonstrate that locating a thin layer of silver catalyst at the external surface of the pellet (surface Dirac-type distribution) provides the optimum selectivity and yield to ethylene oxide. However, this study was conducted without the addition of alkali promoters (11) and organohalide inhibitors (12–14) typically employed in commercial reactors. Addition of chlorine (15, 16) and 1,2-dichloroethane (17) promotes selective ethylene epoxidation over silver catalysts. Depending on the concentration of the chlorine additive, activity promotion, selectivity promotion or poisoning can occur.

In order to reduce catalyst poisoning by 1,2-dichloroethane (DCE), paraffins are added to the feed (18). Ethane is the most effective dechlorinating agent, at least an order of magnitude better than methane and ethylene (19). Alternatively, the addition of alkali compounds can also serve as a buffer for excess chlorine (20).

In the present work, we investigate the effects of DCE addition in the context of optimal silver catalyst distribution for ethylene epoxidation. The performance of uniform and Dirac-type catalysts was examined as a function of DCE

[1] Current Address: Department of Chemical Engineering, Hong Kong University of Science and Technology, H.K.

[2] Current Address: Department of Chemical and Biochemical Engineering, University College London, U.K.

[3] To whom correspondence should be addressed. Fax: 219-631-8366. E-mail: avarma@darwin.cc.nd.edu.

0021-9517/98 $25.00

concentration in the feed and reaction temperature. The influence of ethane addition was also studied.

EXPERIMENTAL

Ethylene oxide is produced by partial oxidation of ethylene over silver catalyst. Complete combustion of ethylene, as well as further oxidation of ethylene oxide to carbon dioxide and water, also occurs during the reaction.

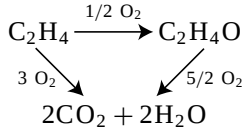

Addition of organohalide inhibitors such as 1,2-dichloroethane can significantly increase the selectivity toward ethylene oxide (17).

Catalyst Pellet

Active powder of stabilized silver catalyst and inert powder of α-alumina were mechanically pressed to form a cylindrical catalyst pellet. The silver catalyst contained 33.8 wt%. Ag supported on α-alumina (Alcoa A-17, 3 m^2/g) and had an active surface area of 0.13 m^2/g catalyst (680-nm crystallites). The inert α-alumina powder was impregnated with sodium hydroxide (0.3 wt%) to reduce its activity toward ethylene oxide combustion and isomerization to acetaldehyde. The details of the preparation procedure are available elsewhere (10).

Catalyst pellets with a narrow step distribution of the active layer were prepared by pressing together one or two layers of inert powder and a layer of active powder in a two-piece die (cf. Fig. 1). The individual layers were pressed at 4000 psi (27 MN/m^2), and the final pellet was pressed at 7000 psi (48 MN/m^2). The cylindrical pellet was 20.4 mm in diameter and 3.6 mm in thickness. The weight of the pellet was kept constant at 2.50 g, with 0.45 g of active powder and 2.05 g of inert powder. Pressing the active powder gives a narrow (0.4 mm) active layer width, which could be positioned at different locations from the surface of the pellet. The thickness of active layer was varied, without changing the catalyst loading, by mixing the active powder with a fraction of the inert powder before pressing into layer form. The cylindrical surface of the pellet was wrapped with Teflon tape and pressed fit into a Teflon sample holder within the reactor. This provided thermal insulation and also restricted the diffusion of reaction gases exclusively through the top surface of the pellet.

Catalyst Characterization

The surface area of silver catalyst both before and after reaction was measured using selective oxygen chemisorption in a dynamic (pulse) chemisorption apparatus at 200°C (21). A monolayer oxygen coverage and one oxygen atom per surface silver atom stoichiometry were expected at this temperature (22). The data from three consecutive chemisorption experiments were reproducible to within 5%. Silver dispersion was calculated from the metal loading measurements conducted in a Perkin–Elmer 2280 flame atomic absorption spectrophotometer. The effects of reaction and the presence of DCE on the surface composition of silver catalysts were determined using X-ray photoelectron spectroscopy (5600 ESCA, Physical Electronics, Inc.).

Ethylene Epoxidation Reaction

Experimental apparatus. The experimental apparatus used has been described previously (10). It included a *single-pellet* reactor, operated under well-mixed conditions using a recycle loop. A gas recycle ratio of 170 was obtained with a two-stage diaphragm pump. Thermocouples were inserted to monitor the temperatures of the reaction mixture just above the pellet, as well as the reactor wall. The latter was used for controlling the reactor temperature.

FIG. 1. Silver catalyst pellet. Dark band is Ag/α-Al_2O_3 and white bands are α-Al_2O_3.

Trace amounts of water present in the feed gases, oxygen (Linde, zero grade), ethylene (Linde, CP grade), and helium (Linde, UHP grade), were removed by moisture traps. The flowrates of the individual gases were metered using Unit UCF-1000 mass flow controllers to give an overall flowrate of 100 ml/min at a fixed gas composition of 6 vol% oxygen, 6 vol% ethylene, and 88 vol% helium (i.e., ethylene-rich conditions). The gases were mixed and preheated to 300°C prior to entering the reactor, which was maintained at 15.6 psi (107 kN/m^2) pressure.

A small portion of the exit gas was drawn off for analysis. A Beckman 565 infrared CO_2 analyzer provided continuos monitoring of carbon dioxide production. Gas composition analysis was performed using a Hewlett–Packard 5890 II gas chromatograph, equipped with both thermal conductivity and flame ionization detectors. The gases were separated by a Porapak-Q column (3.2-mm-OD, 1.8-m-long) at 90°C. The data were collected and analyzed using a Hewlett–Packard 3396 II integrator. Periodic calibrations of the CO_2 analyzer and gas chromatograph were performed to ensure accuracy of the data.

Experimental procedure. The catalyst pellet was aged in the reactor for 24 h at 280°C under inlet reaction feed conditions, and the temperature was then decreased to 210°C where it remained overnight. Data were collected for five different temperatures between 210 and 270°C at 15°C increments. For the study of the effects of DCE, concentrations between 0 and 2 ppm were fed to the reactor, and the role of ethane (0.5 vol%) was also investigated.

No homogeneous or wall reactions were detected for either ethylene or ethylene oxide. Furthermore, the only reaction products were ethylene oxide, carbon dioxide, and water. The catalyst was stable, with no observable change in activity up to 220 h. Each data point reported in this paper is the average of at least three assays made after the reaction had reached steady state and at intervals of about 30 min apart. The maximum variation in these measurements was less than ±3%. The reproducibility for different pellets prepared under identical conditions was excellent, with a maximum variation of 6%. Carbon balances typically closed to within 2%.

Definitions

The overall conversion of ethylene, X, is defined as

$$X = \frac{[(F_{C_2H_4})_{in} - (F_{C_2H_4})_{out}]}{(F_{C_2H_4})_{in}},$$

where F is molar flow rate (gmol/s). The selectivity, S, to ethylene oxide is defined as

$$S = \frac{(F_{C_2H_4O})_{out}}{[(F_{C_2H_2})_{in} - (F_{C_2H_4})_{out}]},$$

and the yield, Y, is

$$Y = XS = \frac{(F_{C_2H_4O})_{out}}{(F_{C_2H_4})_{in}}.$$

The turnover frequency (TOF, molecules/surface Ag atom · s) for ethylene consumption, TOF_E, and productions of carbon dioxide, TOF_{CD}, and ethylene oxide, TOF_{EO}, were calculated from the corresponding mass balances

$$TOF_E = \frac{(F_{C_2H_2})_{in} - (F_{C_2H_2})_{out}}{S_{Ag}} N_{Av}$$

$$TOF_{CD} = \frac{(F_{CO_2})_{out}}{S_{Ag}} N_{Av}$$

$$TOF_{EO} = \frac{(F_{C_2H_4O})_{out}}{S_{Ag}} N_{Av},$$

where S_{Ag} is the number of silver sites (Ag surface atoms) as measured by oxygen chemisorption, and N_{Av} is Avogadro's number (6.02×10^{23} molecules/gmol).

RESULTS AND DISCUSSION

In the present work, the effects of 1,2-dichloroethane addition on the optimal distribution of silver catalyst are investigated. The reaction study is divided into two parts. First, the conversion and selectivity were determined for different levels of DCE (0–2 ppm) in the absence of ethane for three different active layer widths (0.40, 0.90, and 3.6 mm) and three different locations [one surface ($a = 0$) and two subsurface ($a = 0.14$ and 0.64 mm)] of a Dirac-type (0.40-mm-width) catalyst. Second, similar DCE experiments were performed, in the presence of 0.5% ethane in the feed stream, for a uniform (3.6-mm-width) and two Dirac-type ($a = 0$, and 0.64 mm) catalyst pellets.

After the reaction, the catalysts were analyzed using XPS for residual chlorine in the silver catalyst, the presence of carbonaceous deposits (coke), and possible migration of contaminants from the support material. Structural effects of reaction were characterized using oxygen chemisorption and X-ray diffraction.

Ethylene Epoxidation Reaction

The effects of active layer width and location on catalyst performance for ethylene epoxidation reaction are summarized in the selectivity vs conversion plots shown in Figs. 2a and 2b, respectively. Figure 2a demonstrates that both selectivity and conversion decrease with increasing active layer width. The narrow Dirac-type catalyst exhibits the best performance, while the uniform pellet has the lowest selectivity and conversion values. Placing the Dirac-type active layer at subsurface locations reduces catalyst activity and selectivity (cf. Fig. 2b). These results obtained with ethylene-rich feed are in good agreement with previous results obtained under oxygen-rich conditions (10).

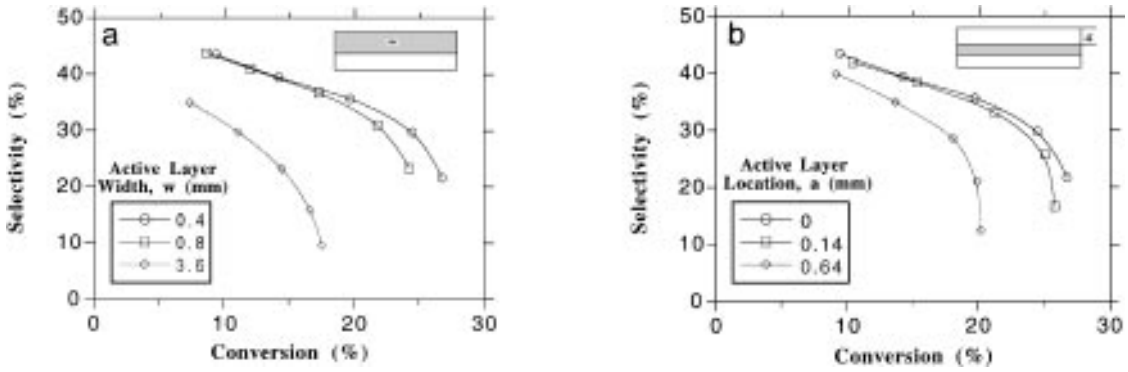

FIG. 2. Selectivity as a function of conversion for various (a) active layer widths and (b) locations within the pellet.

The preceding results indicate that transport resistances, expected to be important for thicker active layer widths and at subsurface locations, are detrimental to both selectivity and conversion. The fact that intraphase oxygen gradients are detrimental to both activity and selectivity is consistent with the observations of previous investigators (23–26), who report that higher oxygen concentrations enhance ethylene oxide yield. In addition, intraphase temperature gradients are also undesirable due to the higher activation energy of ethylene combustion as compared to the ethylene epoxidation reaction (27). Thus, the best performance is achieved by concentrating the active catalyst toward the external surface of the pellet (i.e., a surface Dirac-type distribution).

Effect of 1,2-dichloroethane addition on optimal catalyst profile in pellet. DCE adsorbs on the surface of silver and decomposes to adsorbed chlorine and ethylene (28, 29). Through either electronic or ensemble effects, chlorine affects the oxidation of ethylene over silver catalyst. The influence of DCE feed concentration on the performance of uniform and Dirac-type distributions of catalyst is shown in Fig. 3. Ethylene oxide selectivity for the uniform catalyst (Fig. 3b) increases with DCE addition at low

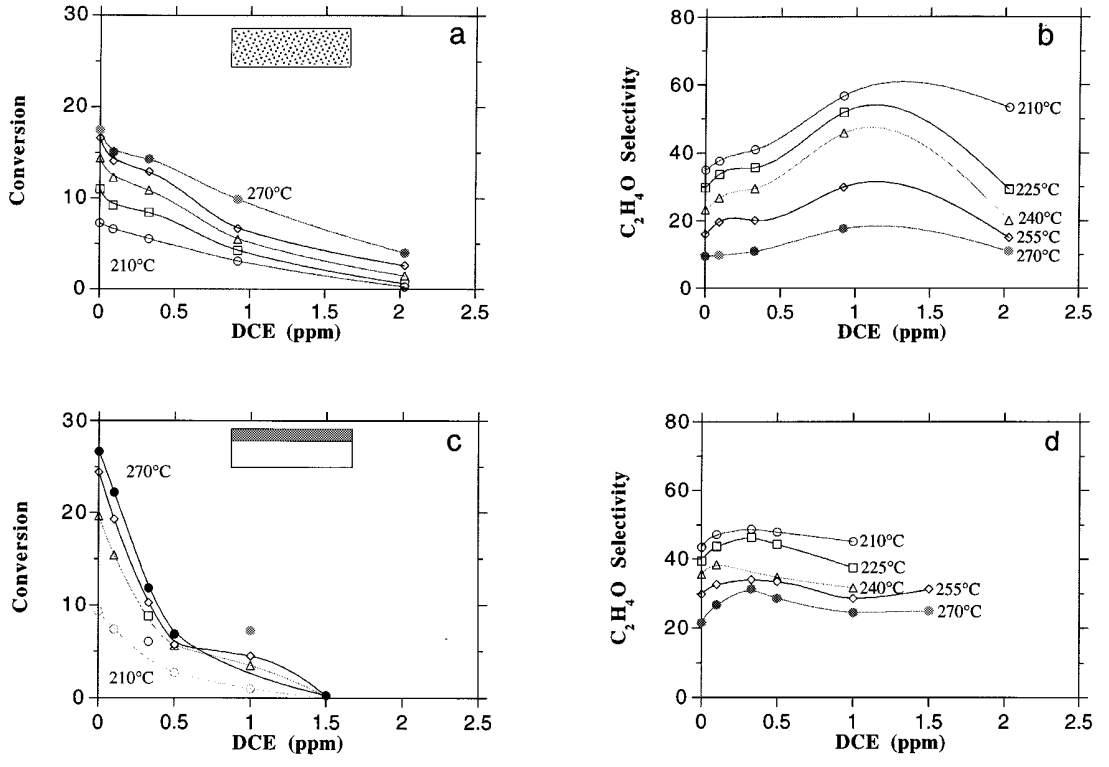

FIG. 3. Conversion and selectivity as a function of DCE concentration and temperature for (a) and (b) uniform and (c) and (d) surface Dirac-type distributions.

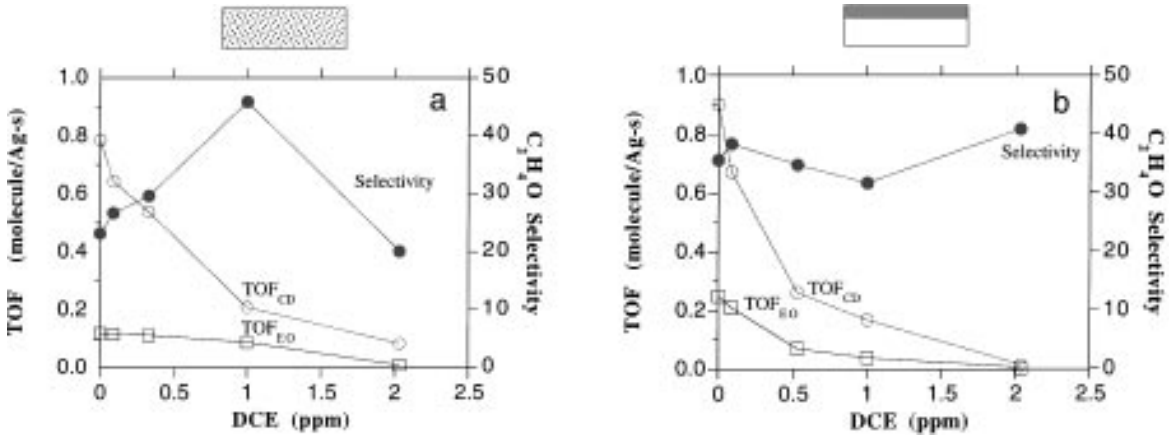

FIG. 4. TOF_{CD}, TOF_{EO}, and selectivity as a function of DCE concentration at $T = 240^{\circ}C$ for (a) uniform and (b) surface Dirac-type distributions.

concentrations, reaching a maximum between 1 and 1.5 ppm. Along with the monotonic decrease in conversion (Fig. 3a), this indicates that addition of DCE promotes catalyst selectivity, but inhibits the overall reaction. The rapid decrease in activity and negligible selectivity enhancement shown in Figs. 3c and 3d, respectively, suggest that the primary effect of DCE addition on the surface Dirac-type catalyst is indiscriminate poisoning of *both* combustion and epoxidation sites.

Figures 4a and 4b show the turnover frequencies for ethylene oxide (TOF_{EO}) and carbon dioxide (TOF_{CD}) production along with selectivity as functions of DCE concentration for the uniform and surface Dirac-type catalysts at 210°C. For both catalysts, TOF_{EO} and TOF_{CD} decrease with increasing DCE levels, which demonstrates that DCE inhibits both epoxidation and combustion reactions. Figure 4a also shows that for a uniform catalyst, DCE at lower levels inhibits combustion to a greater extent than epoxidation, resulting in the observed enhancement of selectivity. No selectivity improvement was observed for surface Dirac-type catalyst (Fig. 4b), indicating that DCE inhibits TOF_{EO} and TOF_{CD} by proportionate amounts.

These observations can be explained by the DCE gradient across the catalyst pellet. In a surface Dirac-type catalyst, the activity is concentrated near the external surface of the pellet where DCE concentration is the highest and in the absence of paraffin leads to catalyst poisoning (18) as shown in Fig. 4b. In a uniform catalyst, the activity is distributed across the pellet where the *average* DCE concentration is less than that at the pellet surface, and the experimental results display a typical inhibition effect with accompanying selectivity promotion (cf. Figs. 3a and 3b). This is in agreement with previous reports that depending on its concentration, DCE can function as selective inhibitor or poison for silver catalyst during ethylene epoxidation (15, 16). It is also well known that chlorine can accumulate in the silver catalyst after prolonged exposure to DCE (11). In order to minimize this effect, the experiments were conducted at a fixed DCE level and the temperature dependence was determined. During the 12-h period of the experiment for DCE < 1.5 ppm, there was no significant difference between the initial and final catalyst activity and selectivity. However, for DCE ≥ 1.5 ppm, a 10–25% decrease in catalyst performance was observed.

Figure 5 demonstrates that the choice of catalyst distribution depends on the performance index and the DCE level. The selectivity, conversion, and yield are shown as a function of reaction temperature for surface Dirac-type and uniform catalysts. In the absence of DCE (cf. Fig. 5a), the surface Dirac-type catalyst has better conversion, selectivity, and yield as compared to the uniform catalyst. The same observation is also true for a relatively low DCE concentration of 0.1 ppm (Fig. 5b). At higher DCE concentration (0.33 ppm), the conversion for the surface Dirac-type catalyst is lower than the uniform, but both selectivity and yield are higher, as shown in Fig. 5c. Finally, the uniform catalyst has better conversion and yield as compared to the surface Dirac-type catalyst at DCE level of 1 ppm (cf. Fig. 5d). In addition, it has higher selectivity for ethylene oxide at low reaction temperatures.

The preceding results suggest that a subsurface location of Dirac-type catalyst could provide better reaction performance. Figure 6 shows the conversion and selectivity as a function of DCE concentration and reaction temperature for two subsurface locations, $a = 0.14$ mm (Figs. 6a and 6b) and $a = 0.64$ mm (Figs. 6c and 6d). Figures 6a and 6c (compare with Fig. 3c) indicate that the reaction inhibition (i.e., decrease in conversion) occurs at higher concentrations as the active layer is located within the pellet. As a consequence, they exhibit slight conversion plateaus at low DCE concentrations (0–0.5 ppm). But, more importantly, the subsurface catalysts exhibit higher selectivity enhancement (Figs. 6b and 6d) which is essentially absent in the surface Dirac-type catalyst (cf. Fig. 3d).

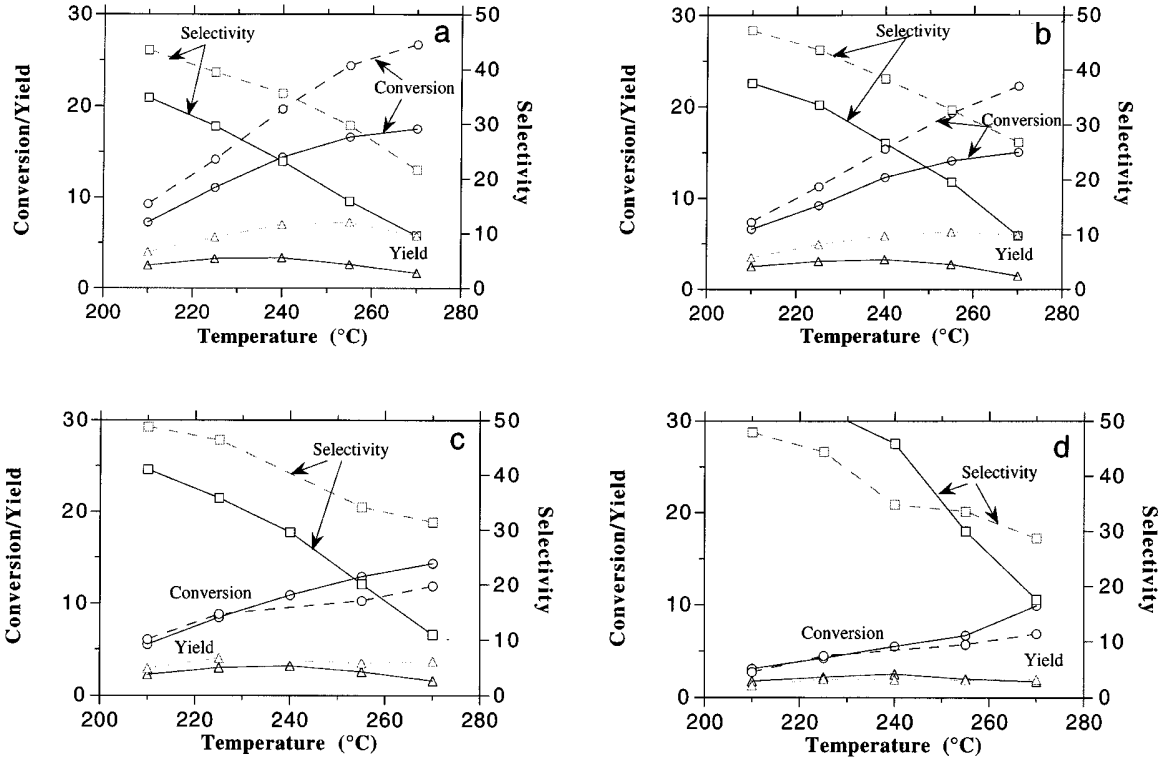

FIG. 5. Conversion, selectivity, and yield versus temperature plots of uniform (solid line) and surface (dashed line) Dirac-type catalysts for DCE feed concentrations of (a) 0, (b) 0.1, (c) 0.3, and (d) 1 ppm.

Due to transport resistances, the concentration of DCE decreases along the depth of the pellet. An active layer placed at subsurface locations (cf. Fig. 6) is exposed to a lower concentration of DCE as compared to the surface Dirac-type catalyst. This gives rise to the desired inhibition effect that enhances selectivity, while preventing catalyst poisoning which occurs at higher DCE concentrations. However, there is a tradeoff in that the conversion (e.g., $T = 270°C$) decreases from surface to subsurface locations (cf. Figs. 3c, 6a, and 6c). This is caused by the lower reactant (i.e., ethylene and oxygen) concentrations within the pellet and further combustion of ethylene oxide, which are consistent with the results shown in Fig. 2b.

The aforementioned change in the conversion–DCE and selectivity–DCE plots (Fig. 6) is quite significant if we take into consideration that the subsurface locations of the active layer are relatively shallow, 0.14 and 0.64 mm, which are about 4 and 18% of the pellet characteristic length, respectively. This effect is especially pronounced for the case of $a = 0.14$ mm. An examination of Fig. 2b shows that in the absence of DCE, the performances of the surface and subsurface ($a = 0.14$ mm) Dirac-type catalysts are essentially identical at temperatures less than 255°C. However, this thin diffusion barrier is sufficient to reduce catalyst poisoning by DCE, resulting in a significant selectivity promotion. For this reason, the subsurface catalyst has better performance.

Figure 7 shows the turnover frequencies for carbon dioxide (TOF_{CD}) and ethylene oxide (TOF_{EO}) productions of the uniform (Figs. 7a and 7b), surface Dirac-type (Figs. 7c and 7d), and subsurface ($a = 0.64$ mm) Dirac-type (Figs. 7e and 7f) catalysts, as a function of reaction temperature and DCE concentration. For the three catalyst distributions and locations, TOF_{CD} increases with increasing temperatures and decreases with increasing DCE concentrations (cf. Figs. 7a, 7c, and 7e). The presence of maxima in the TOF_{EO}–temperature curves (cf. Figs. 7b, 7d, and 7f) indicates either that ethylene oxide combustion may be occurring or that the intraphase concentrations of reactants were significantly decreased. For both uniform and surface Dirac-type catalysts, TOF_{EO} decreases with increasing DCE levels. TOF_{EO} decreases by a lesser extent than TOF_{CD} for the uniform distribution, whereas TOF_{EO} for the surface Dirac-type distribution decreases by the same extent as TOF_{CD}, thus yielding the selectivity performance shown in Figs. 3b and 3d. At low DCE concentrations (≤ 0.5 ppm), TOF_{EO} for the subsurface Dirac-type distribution increases with DCE addition. The change in the shape of TOF_{EO}–temperature curves with the addition of DCE indicates that DCE also inhibits ethylene oxide combustion.

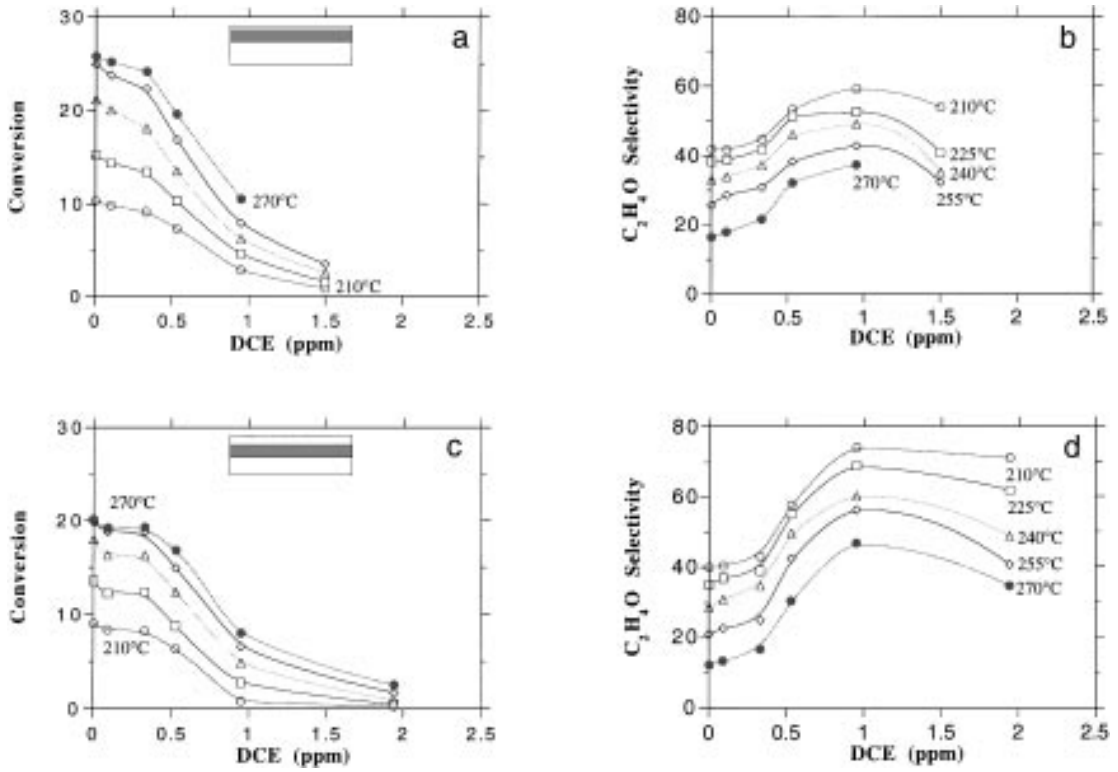

FIG. 6. Conversion and selectivity as a function of DCE concentration and temperature for Dirac-type catalysts located at (a) and (b) $a = 0.14$ and (c) and (d) $a = 0.64$ mm from the surface.

The role of ethane in ethylene epoxidation reaction. As noted earlier, decomposition of DCE yields adsorbed chlorine. Its accumulation can result in formation of bulk silver chloride which can alter the topology of the active surface and diminish catalyst activity (11). The presence of ethane can effectively depress the steady-state concentration of adsorbed chlorine by reacting with it (18).

For this study, three different catalyst pellets were prepared: a uniform and two Dirac-type ($a = 0$ and 0.64 mm) pellets. First, for each pellet, the conversion and selectivity were measured in the absence of DCE and ethane. The pellets were then exposed to 6 vol% ethylene, 6 vol% oxygen, 0.5 vol% ethane, and balance helium at 240°C for 12 h. This treatment ensures the removal of trace chlorine that may be present in the catalyst due to contamination from the atmosphere. The post-treatment conversion and selectivity were then measured. The data obtained before and after the treatment were within the experimental error of 5%, indicating that the initial silver catalyst was free of chlorine. In addition, the selectivity of the catalyst (43%) was within the range of values for clean single crystal Ag catalyst (30–42%) [30, 31].

Figures 8a–8d demonstrate that the addition of 0.5 vol% ethane in the feed significantly alters the performance of both uniform and surface Dirac-type catalysts. The decrease in conversion (cf. Figs. 8a and 8c) occurs at higher feed concentrations of DCE for both catalysts and at a slower rate as compared to the previous results obtained in the absence of ethane (cf. Fig. 3). In addition, *both* catalysts display selectivity enhancement with addition of DCE (cf. Figs. 8b and 8d) and the measured enhancements are larger as compared to those of Figs. 6b and 6d. For example, at 1.5 ppm DCE and 210°C, the selectivity for the uniform catalyst is 65%, while for the surface Dirac-type catalyst, it is about 72%. The subsurface location of catalyst (Fig. 8e and 8f) yields conversions intermediate between surface and uniform distributions, while the selectivity values are somewhat better, particularly at lower DCE levels.

The conversion data shown in Figs. 8a and 8c display a strong resemblance to those of Figs. 6a and 6c. This suggests that the addition of 0.5 vol% ethane has the same effect as placing the active layer at subsurface locations. In both cases, the amount of adsorbed chlorine is decreased either by reaction with ethane or by the decrease in local concentration of DCE due to transport limitations. The use of ethane is more advantageous, for it avoids the negative effects associated with placing the catalyst at interior locations, such as ethylene oxide combustion which reduces catalyst selectivity, and lower reactant concentrations (ethylene and oxygen) which are detrimental to both conversion and selectivity. The performance of the surface Dirac-type catalyst in the presence of ethane (Figs. 8c and

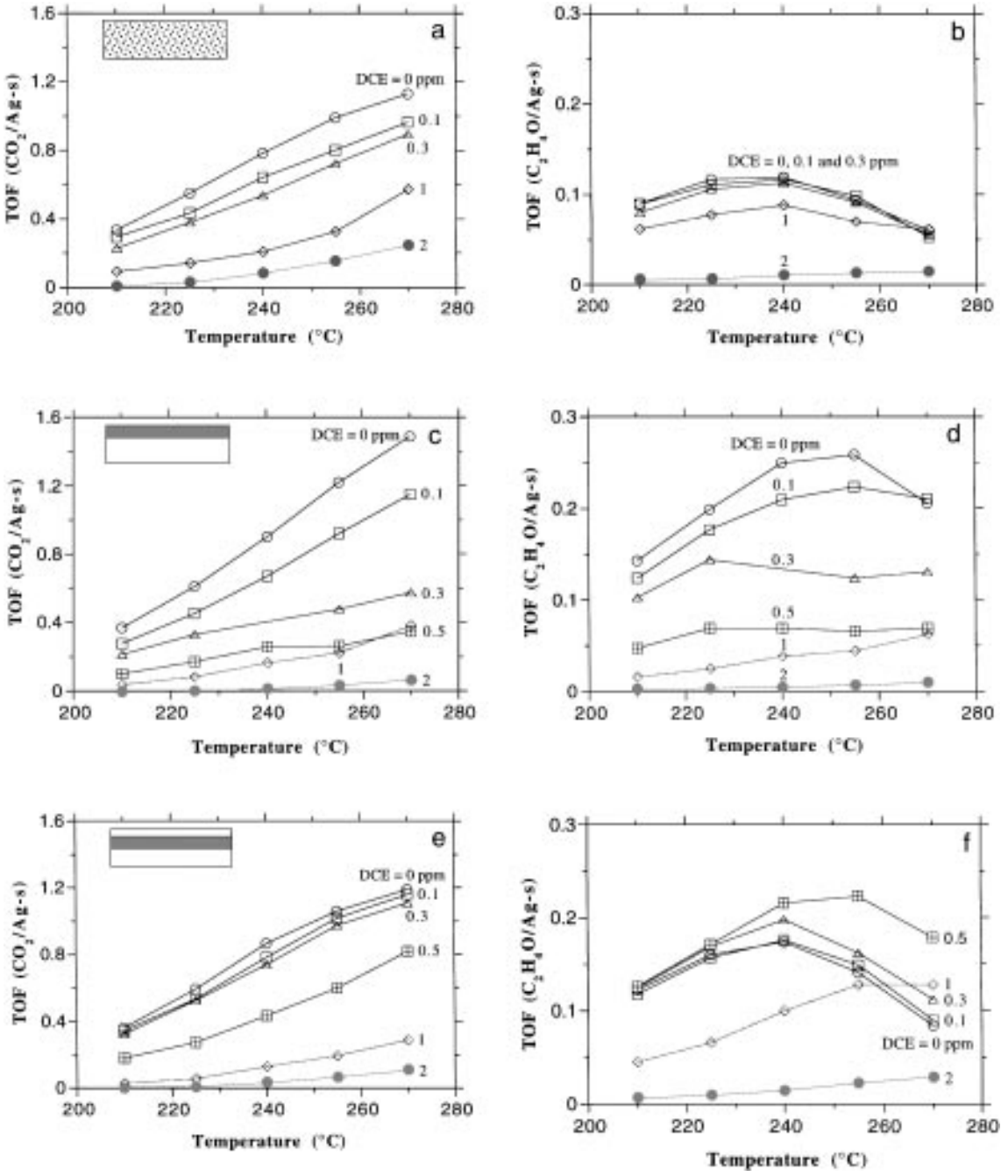

FIG. 7. Net reaction rates (TOF_{CD} and TOF_{EO}) as a function of temperature and DCE concentration for (a) and (b) uniform, (c) and (d) surface Dirac-type ($a = 0$ mm), and (e) and (f) subsurface Dirac-type ($a = 0.64$ mm) catalyst pellets.

8d) is superior as compared to both subsurface catalysts shown in Fig. 6.

The above results can be conveniently summarized in the plots of selectivity at a constant conversion (10%) as a function of DCE concentration, for the different active catalyst distributions investigated in this work. The results for 0 and 0.5 vol% ethane are shown in Figs. 9a and 9b, respectively. Both figures indicate that a nonuniform distribution of catalyst has better selectivity (hence yield) than the uniform catalyst. Low concentrations of DCE improve catalyst selectivity, while higher concentrations are detrimental. A surface Dirac-type catalyst has better performance at low DCE levels ($\leq$0.2 ppm). However, enhanced selectivity is attained at higher DCE levels (0.7–1.5 ppm) for subsurface Dirac-type catalysts. In particular, the broad maximum displayed by the subsurface Dirac-type catalyst in the presence

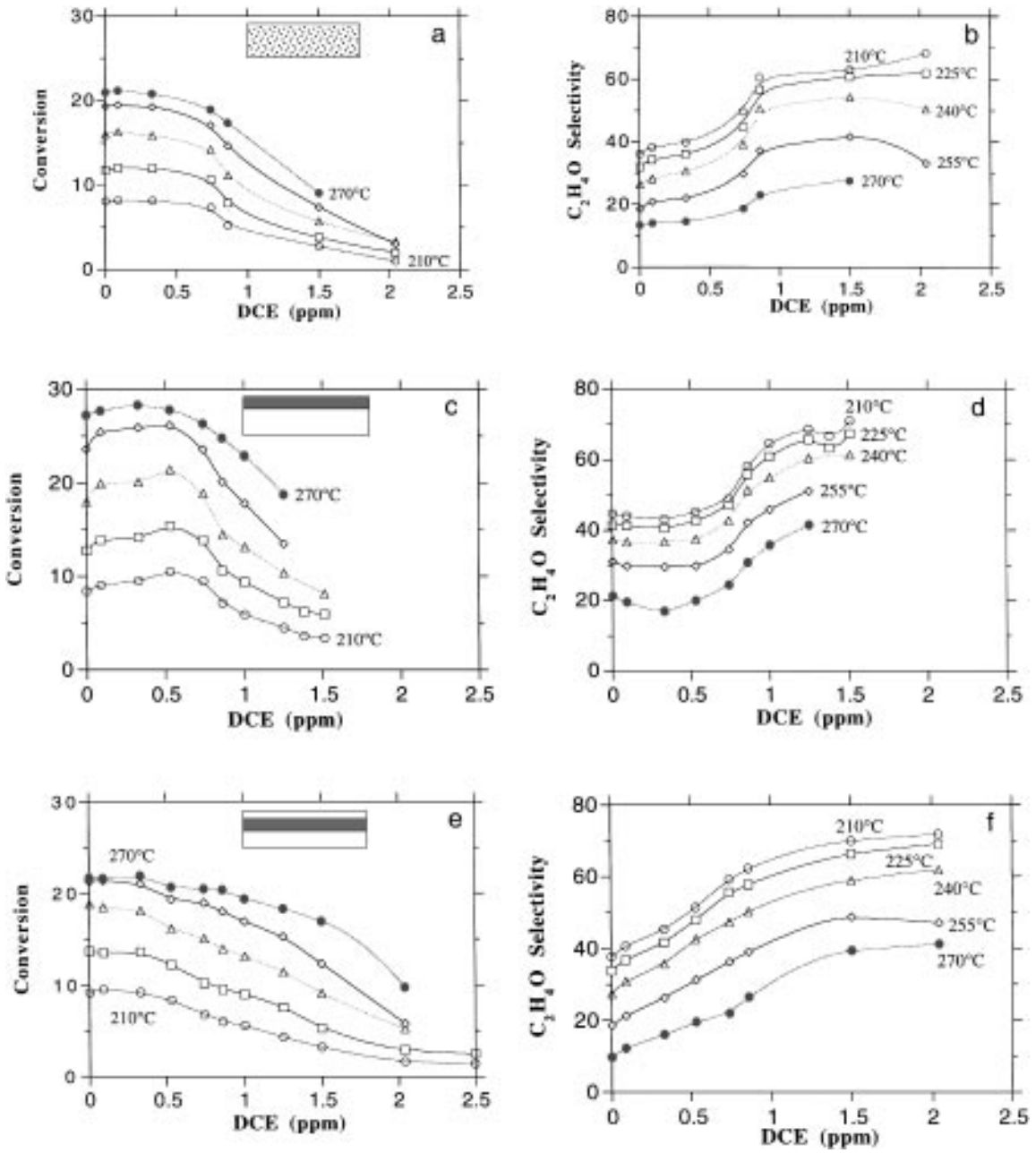

FIG. 8. Conversion and selectivity as a function of DCE concentration and temperature for (a) and (b) uniform, (c) and (d) surface Dirac-type, and (e) and (f) subsurface Dirac-type ($a = 0.64$ mm) distributions.

of ethane allows a larger window of operation and greater tolerance for fluctuations in the feed DCE concentrations.

Catalyst Characterization

In the absence of DCE, the shape of the selectivity–conversion plots shown in Fig. 2 is typical of ethylene epoxidation reaction and is independent of the catalyst distribution. Addition of DCE without ethane results in a change of the curve shape caused by both decrease in conversion due to poisoning and increase in selectivity due to promotion (Fig. 10). Similar behavior is also observed in the presence of ethane, but the changes are less pronounced and occur at higher DCE concentrations. This change in the shape of the selectivity–conversion curve reflects changes in the catalytic surface during reaction. The observed decrease in activity can be caused by either sintering or formation of inactive bulk silver chloride, which reduce the *physical* surface area of the catalyst. It can also be caused by deposition

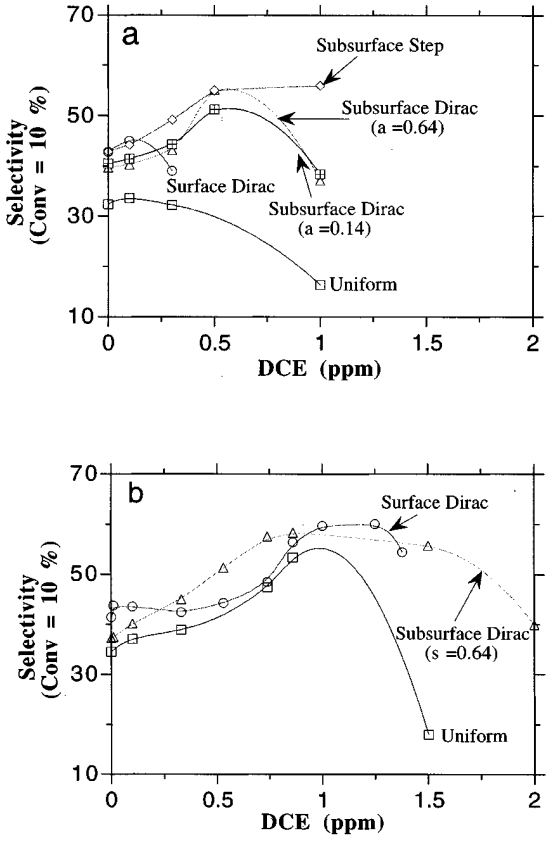

FIG. 9. Ethylene oxide selectivity as a function of DCE concentration at a fixed 10% ethylene conversion for various distributions of catalyst, (a) ethane = 0, and (b) ethane = 0.5%.

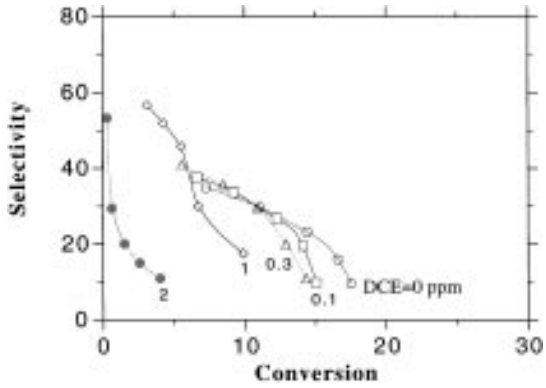

FIG. 10. Selectivity as a function of conversion and DCE concentration for a uniform catalyst pellets.

of carbon and chlorine, which can block the active sites.

Measurements of silver surface area were conducted before and after reaction using oxygen chemisorption. In the absence of DCE and ethane, the catalyst surface area remained constant throughout the experiment. This was confirmed by the reproducibility of the conversion and selectivity data, and shows that the catalytic surface was fully stabilized using the pretreatment procedure outlined in the experimental section. Catalysts exposed to DCE during reaction exhibited poisoning which was significantly decreased by the addition of ethane. Spent catalysts from these experiments were pretreated under reactant stream containing ethane (DCE = 0) prior to the chemisorption study. This procedure effectively removes surface chlorine and recovers the initial catalyst activity, as also reported by Endler (19). The surface area of the spent catalyst after this pretreatment was essentially the same as that of the fresh catalyst, indicating that although the active surface area changes in the presence of DCE, no physical sintering occurred under these reaction conditions.

X-ray diffraction studies revealed peaks corresponding only to silver and α-alumina for both fresh and spent catalysts. Diffraction lines corresponding to bulk silver chloride were not detected. This suggests either that there is no formation of bulk silver chloride crystals or that its amount is below detection limits.

TABLE 1

XPS Data for Fresh and Spent Silver Catalyst

Sample	Depth (Å)	Al	O	Ag	C	Na	Cl	S	F	Si	Fe	N
α-Al_2O_3 support (A1)	15	33.60	59.30	—	0.59	5.90	—	0.11	0.14	0.13	0.04	0.22
	70	33.90	59.90	—	0.46	5.40	—	—	0.16	0.09	0.03	—
Fresh Ag/α-Al_2O_3 (A2)	15	25.52	48.10	4.12	19.80	2.20	0.12	—	—	0.18	—	—
	70	28.12	49.60	4.84	14.10	2.20	0.20	—	—	0.42	—	—
Spent surface Dirac-type catalyst	15	27.29	47.40	2.48	17.50	2.40	0.15	0.45	1.20	0.86	—	0.38
(w/o ethane) (S1)	70	27.80	50.30	2.59	13.80	2.30	0.16	0.53	1.01	1.14	—	0.45
Spent surface Dirac-type catalyst	15	26.11	51.50	3.43	12.50	2.30	0.01	0.82	0.41	2.31	—	0.58
(w/o ethane) (S2)	70	27.23	52.80	3.74	10.90	1.93	0.06	0.76	0.32	2.04	—	0.25
Spent subsurface Dirac-type	15	28.68	48.24	4.84	13.55	2.99	0.45	0.10	0.22	0.65	—	0.60
catalyst (w/o ethane) (S3)	70	29.86	48.91	4.69	11.82	3.19	0.60	0.20	0.12	0.52	—	0.53

X-ray photoelectron spectroscopy was conducted on both the fresh and the spent catalyst samples, and the results are summarized in Table 1. Two angles of incidence were employed, 15 and 80°, to obtain the corresponding penetration depths of 15 and 70 Å, respectively, which provide information on both the surface and bulk compositions of the catalyst. The α-alumina powder (A1) contains sodium, carbon, fluorine, and silicon as main impurities arising from the manufacturing and pelletizing steps. Trace amounts of iron and sulfur were also detected. The fresh silver catalyst powder (A2) shows a significant deposit of carbon and trace amounts of chlorine. The carbon probably resulted from decomposition of lactic acid used in the catalyst preparation. Sodium present in the catalyst originated from the support. Since sodium is also a promoter (32), this may influence the performance of the *fresh* catalyst.

XPS analysis of the two surface Dirac-type catalysts (S1 and S2) employed in the experiments (Figs. 3c and 3d and Figs. 8c and 8d, respectively) demonstrates that the addition of ethane (S2) significantly reduces both surface and subsurface chlorine. The similarity of the surface and subsurface chlorine signals for the S1 catalyst suggests that bulk silver chloride is present for the silver exposed to DCE in the absence of ethane (cf. S2 in Table 1). It was shown in the preceding section that besides addition of ethane, placing the active layer at subsurface locations can also retard catalyst poisoning. The composition of such a catalyst (S3) is shown in Table 1. The analysis shows a higher chlorine content as compared to both surface Dirac-type catalysts (S1 and S2), probably because this catalyst was exposed to higher DCE levels during the reaction experiments.

The XPS data also indicate the presence of sulfur in both the support A1 and spent catalysts (S1–S3). Sulfur exists as SO_4^{2-} contaminant in the alumina support as received. Examining sample A2 indicates that sulfur in the spent catalysts (S1–S3) is due to contamination from the hydrocarbon feedstocks. It is interesting to note that in the subsurface catalyst (S3), sulfur is significantly lower than in either surface catalysts (S1, S2). This demonstrates that the presence of a diffusion barrier can significantly prevent undesirable contaminants from reaching the active catalyst. The fluorine signal measured from the spent catalysts is likely due to the Teflon wrapping employed in the experiments. The relatively fixed value of sodium signal indicates that there is no significant migration of sodium from the surrounding α-alumina.

CONCLUDING REMARKS

In the present work, it has been demonstrated that for ethylene epoxidation, the choice of silver catalyst distribution in pellets depends on the performance index (i.e., conversion, selectivity, and yield) being optimized, the DCE level, and the presence of ethane in the feed. In the absence of DCE and ethane, a surface Dirac-type catalyst pellet exhibits high ethylene conversion, as well as high selectivity and yield toward ethylene oxide. In the presence of DCE, with or without ethane, a subsurface Dirac-type distribution has the best selectivity and yield. In general, a nonuniform distribution of silver catalyst exhibits better performance than a uniform distribution.

Catalyst characterization studies indicate that loss of activity in the presence of DCE is reversible and is not caused by sintering of silver crystallites. Formation of subsurface chlorides is apparent from the XPS analysis of catalysts (S1 and S3) exposed to DCE in the absence of ethane. Placing the active layer at a subsurface location (S3) significantly reduces the amount of contaminants (e.g., S) reaching the silver catalyst.

ACKNOWLEDGMENTS

We gratefully acknowledge financial support from the Union Carbide Corporation. We also thank Dr. Ghaleb N. Salaita of Union Carbide for conducting the XPS analysis.

REFERENCES

1. Wu, H., Brunovska, A., Morbidelli, M., and Varma, A., *Chem. Eng. Sci.* **45**, 1855 (1990).
2. Brunovska, A., Morbidelli, M., and Brunovsky, P., *Chem. Eng. Sci.* **45**, 917 (1990).
3. Morbidelli, M., Servida, A., and Varma, A., *Ind. Eng. Chem. Fundam.* **21**, 278 (1982).
4. Gavriilidis, A., Varma, A., and Morbidelli, M., *Catal. Rev.-Sci. Eng.* **35**, 399 (1993).
5. Chemburkar, R. M., "Optimal Catalyst Activity Profiles in Pellets: Single Pellet Theory and Experiments," Ph.D. Thesis, University of Notre Dame (1987).
6. Lee, C. K., and Varma, A., *Chem. Eng. Sci.* **43**, 1995 (1988).
7. Masi, M., Sangalli, M., Carra, S., Cao, G., and Morbidelli, M., *Chem. Eng. Sci.* **43**, 1849 (1988).
8. Wu, H., Yuan, Q., and Zhu, B., *Ind. Eng. Chem. Res.* **27**, 1169 (1988).
9. Wu, H., Yuan, Q., and Zhu, B., *Ind. Eng. Chem. Res.* **29**, 1771 (1990).
10. Gavriilidis, A., and Varma, A., *AIChE J.* **38**, 291 (1992).
11. Berty, J. M., "Ethylene Oxide Synthesis," *in* Applied Industrial Catalysis, Vol.1, Academic Press, New York, 1983.
12. Law, G. H., and Chitwood, H. C., U.S. Patent 2,194,602 (1940).
13. Law, G. H., and Chitwood, H. C., U.S. Patent 2,279,469 (1942).
14. Ostrovskii, N. V., Kulkova, N. V., Lopatin, V. L., and Temkin, M. I., *Kinet. Catal.* **3**, 160 (1962).
15. Campbell, C. T., and Koel, B. E., *J. Catal.* **92**, 272 (1985).
16. Campbell, C. T., *J. Catal.* **99**, 28 (1986).
17. Rovida, G., Pratesi, F., and Ferroni, E., *J. Catal.* **41**, 140 (1976).
18. McKim, F. L. W., and Cambron, A., *Can. J. Res.* **B27**, 813 (1949).
19. Endler, H., Italian Patent 600,389 (1959).
20. Bhasin, M. M., Ellgen, P. C., and Hendrix, C. H., U.K. Patent Application 2,043,481 (1980).
21. Gavriilidis, A., Sinno, B., and Varma, A., *J. Catal.* **139**, 41 (1993).

22. Czanderna, A. W., *J. Phys. Chem*. **68**, 2765 (1964).
23. Gavriilidis, A., "Optimal Distribution of Silver Catalyst in Pellets for Epoxidation of Ethylene," Ph.D. Thesis, University of Notre Dame (1993).
24. Murray, K. E., *Austral. J. Sci. Res.* **A3**, 433 (1950).
25. Wan, S.-W., *Ind. Eng. Chem*. **45**, 234 (1953).
26. Guseinov, S. L., Frolkina, I. T., Vaselivich, L. A., Avetisov, A. K., and Gelbshtein, A. I., *Kin. Catal.* **18**, 895 (1977).
27. Van Santen, R. A., and Kuipers, H. P. C. E., *Adv. Catal.* **35**, 265 (1987).
28. Margolis, L. Ya., *Adv. Catal.* **14**, 429 (1963).
29. Stepanov, Yu. N., Margolis, L. Ya., and Roginskii, S. Z., *Kinet. Katal.* **2**, 684 (1960).
30. Kummer, J. T., *J. Phys. Chem*. **60**, 666 (1956).
31. Campbell, C. T., *J. Catal.* **94**, 436 (1985).
32. Finch, H. V., U.S. Patent 2,424,083 (1947).